Eur. Phys. J. D **12**, 499–508 (2000)

THE EUROPEAN PHYSICAL JOURNAL D

EDP Sciences

Noiseless amplification of images in a confocal cavity

S. Mancini[1], A. Gatti[1,a], and L. Lugiato[2]

[1] INFM, Dipartimento di Fisica, Università di Milano, Via Celoria 16, 20133 Milano, Italy
[2] INFM, Dipartimento di Scienze Chimiche e Matematiche, Università dell'Insubria, Via Lucini 3, 22100 Como, Italy

Received 23 March 2000

Abstract. We study the noiseless amplification of an optical image by means of a confocal cavity containing a parametric medium. We demonstrate, in the ideal situation, the possibility of preserving the signal-to-noise ratio while amplifying uniformly the entire image. Some specific effects, which may degrade the performances of the scheme, are taken into account.

PACS. 42.50.Ar Photon statistics and coherence theory – 42.50.Lc Quantum fluctuations, quantum noise, and quantum jumps – 42.65.Yj Optical parametric oscillators and amplifiers

1 Introduction

The subject of noiseless amplification of optical images belongs to the latest developments in the area of quantum optics. It aims to extend to the spatial domain the possibility of noiseless amplification of temporal optical signals [1]. The first step towards a noiseless image amplifier was made in [2], showing that such a device can be realized by a planar-cavity optical parametric oscillator below threshold operating as a phase-sensitive amplifier. More recently, the traveling-wave version of the parametric image amplifier, has been studied [3,4]. However, both schemes are limited by the fact that the amplification takes place in a non uniform way over the spatial extent of the image. As a consequence the noiseless character of the amplification strongly depends on the point in the transverse plane.

Here, instead, we propose a modification of the model of reference [2] in order to have a spatial uniform performance. This is simply obtained by means of a confocal cavity. In this case only deviations from the ideal situation lead to non-uniform transverse effects. To this end we investigate the influence of finite size pump, phase mismatch between signal and pump, non perfect resonance between signal and cavity, and deviation from confocality.

On the other hand, recently, the traveling-wave parametric image amplification has been investigated experimentally, both at a classical [5] and at a quantum level [6, 7]. In particular, in [7] noiseless image amplification was observed for the first time. Hence, our results could be useful for experimental research in the field of generation, detection and amplification of low-noise optical images.

The paper is organized as follows. In Section 2 we describe the optical scheme. In Section 3 we study the light field dynamics. In Section 4 we investigate the gain and the noise characteristics of the system. In Section 5 we establish conditions for noiseless amplification. Section 6 includes the effects of non ideal situation. Section 7 concludes.

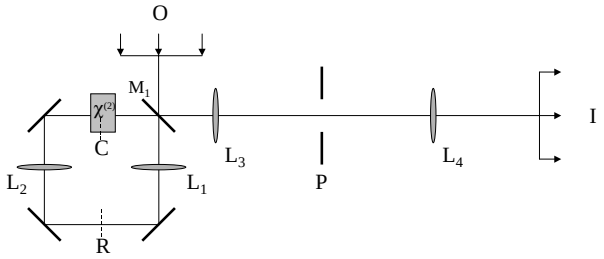

Fig. 1. Optical scheme of the parametric image amplifier with confocal cavity. The latter consists of a ring resonator containing two equal lenses whose focal length f is one fourth of the cavity round trip length. Mirror M_1 has non-zero transmittivity, while the others are totally reflecting at the signal wavelength. All the distances O−L_1, L_1−R, R−L_2, L_2−C, C−L_1, C−L_3, L_3−P, P−L_4, L_4−I are equal to f.

2 The optical scheme

The optical scheme we consider is shown in Figure 1. A faint image which is to be amplified is located in the object plane; this image is projected by the lenses L_1 and L_2 in a $\chi^{(2)}$ nonlinear crystal placed inside the cavity. The amplified image is then projected in the image plane by the other two lenses L_3 and L_4. For the sake of simplicity, we take all the lenses with the same focal length f. We consider a ring cavity configuration with plane mirrors, containing two lenses placed at a distance $2f$ apart. This configuration is equivalent to a Fabry-Perot confocal

[a] e-mail: alessandra.gatti@mi.infn.it

cavity made of two spherical mirrors of radius of curvature $R = 2f$ separated by a distance R. We also consider the presence of a pupil of finite area between the lenses L_3 and L_4. Introduction of a pupil of finite size is necessary for evaluation of the noise properties of the system. The amplified image is detected by a dense array of small photodetectors (pixels) in the image plane.

Let $a(\boldsymbol{\rho}, t)$ and $a^\dagger(\boldsymbol{\rho}, t)$ be the radiation field operators in the object plane. Here, the two-component vector $\boldsymbol{\rho} = (x, y)$ indicates the position in the transverse plane, *i.e.* the plane orthogonal to the mean direction of propagation z. The field operators obey the free-field commutation relation

$$\left[a(\boldsymbol{\rho}, t), a^\dagger(\boldsymbol{\rho}', t)\right] = \delta\left(\boldsymbol{\rho} - \boldsymbol{\rho}'\right)\delta\left(t - t'\right), \tag{1}$$

and are normalized so that $\langle a^\dagger(\boldsymbol{\rho}, t)a(\boldsymbol{\rho}, t)\rangle$ gives the mean value of the source irradiance at the object plane (expressed in photons per cm^2 per second).

We denote the corresponding operators in the image plane as $e(\boldsymbol{\rho}, t)$ and $e^\dagger(\boldsymbol{\rho}, t)$. The relevant observable is the surface photocurrent density $i(\boldsymbol{\rho}, t)$ (that is the number of photoelectrons per cm^2 per second without multiplication by the charge of electron). The mean value $\langle i(\boldsymbol{\rho}, t)\rangle$ of the photocurrent density and its correlation function $\langle \delta i(\boldsymbol{\rho}, t), \delta i(\boldsymbol{\rho}', t')\rangle$, where $\delta i(\boldsymbol{\rho}, t) = i(\boldsymbol{\rho}, t) - \langle i(\boldsymbol{\rho}, t)\rangle$, are given by the quantum theory of photodetection [8]

$$\langle i(\boldsymbol{\rho}, t)\rangle = \eta\langle e^\dagger(\boldsymbol{\rho}, t)e(\boldsymbol{\rho}, t)\rangle, \tag{2}$$

$$\begin{aligned}\langle \delta i(\boldsymbol{\rho}, t), \delta i(\boldsymbol{\rho}', t')\rangle &= \langle i(\boldsymbol{\rho}, t)\rangle\delta\left(\boldsymbol{\rho} - \boldsymbol{\rho}'\right)\delta\left(t - t'\right) \\ &+ \eta^2\big[\langle : e^\dagger(\boldsymbol{\rho}, t)e(\boldsymbol{\rho}, t)e^\dagger(\boldsymbol{\rho}', t')e(\boldsymbol{\rho}', t') : \rangle \\ &- \langle e^\dagger(\boldsymbol{\rho}, t)e(\boldsymbol{\rho}, t)\rangle\langle e^\dagger(\boldsymbol{\rho}', t')e(\boldsymbol{\rho}', t')\rangle\big]. \end{aligned} \tag{3}$$

Here η is the quantum efficiency of a pixel and the symbol $: \ldots :$ indicates normal ordering.

The correlation function (3) contains two contributions. The first one is given by the term

$$\sim \delta\left(\boldsymbol{\rho} - \boldsymbol{\rho}'\right)\delta\left(t - t'\right)$$

and represents the shot noise; it does not depend on the statistics of the light and is proportional to the mean irradiance in the image plane. The second contribution is given by a fourth-order field correlation function, describing normally ordered intensity correlations of the light field. This term accounts for the statistical properties of the light, both in the spatial and in the temporal domain.

We take into account the finite area S_d of the pixels, and that the photocurrent from each pixel is collected during the observation time T_d. Thus, the quantity of interest is the number of photodetections $N_\mathrm{I}(\boldsymbol{\rho}, t)$ registered by the pixel centered at the point $\boldsymbol{\rho}$ in the image plane in the time window $[t - T_\mathrm{d}/2, t + T_\mathrm{d}/2]$, that is

$$N_\mathrm{I}(\boldsymbol{\rho}, t) = \int_{S_\mathrm{d}} \mathrm{d}\boldsymbol{\rho}' \int_{T_\mathrm{d}} \mathrm{d}t'\, i(\boldsymbol{\rho}', t'). \tag{4}$$

We consider the mean number $\langle N_\mathrm{I}(\boldsymbol{\rho}, t)\rangle$ of registered electrons as the amplified signal of our scheme. Its variance

$$\begin{aligned}\langle \Delta N_\mathrm{I}^2(\boldsymbol{\rho}, t)\rangle = \int_{S_\mathrm{d}} \mathrm{d}\boldsymbol{\rho}' \int_{T_\mathrm{d}} \mathrm{d}t' \int_{S_\mathrm{d}} \mathrm{d}\boldsymbol{\rho}'' \\ \times \int_{T_\mathrm{d}} \mathrm{d}t''\langle \delta i(\boldsymbol{\rho}', t'), \delta i(\boldsymbol{\rho}'', t'')\rangle, \end{aligned} \tag{5}$$

characterizes the noise properties of the amplified image; the power signal-to-noise ratio (SNR) of the amplified image is given by [9]

$$R_\mathrm{I} = \frac{\langle N_\mathrm{I}(\boldsymbol{\rho}, t)\rangle^2}{\langle \Delta N_\mathrm{I}^2(\boldsymbol{\rho}, t)\rangle}\ . \tag{6}$$

The equivalent quantities $\langle N_\mathrm{O}(\boldsymbol{\rho}, t)\rangle$, $\langle \Delta N_\mathrm{O}^2(\boldsymbol{\rho}, t)\rangle$ and R_O, measured in the object plane, describe the signal and the noise of the input image. For a stationary signal all these quantities do not depend on time. Our purpose is to compare R_I and R_O and to show that under proper circumstances they can stay equal: we refer to this situation as *noiseless amplification*.

Using equations (4, 5) together with the photodetection formulas (2, 3) we can express $\langle N_\mathrm{I}(\boldsymbol{\rho}, t)\rangle$ and $\langle \Delta N_\mathrm{I}^2(\boldsymbol{\rho}, t)\rangle$ through the mean irradiance $\langle e^\dagger(\boldsymbol{\rho}, t)e(\boldsymbol{\rho}, t)\rangle$ and the intensity correlation function $\langle e^\dagger(\boldsymbol{\rho}, t)e^\dagger(\boldsymbol{\rho}', t')$ $\times e(\boldsymbol{\rho}', t')e(\boldsymbol{\rho}, t)\rangle$ of the field in the image plane. To evaluate these quantities in terms of the input signal and the gain of the amplifier we need the relation between the field operators in the image plane and those in the object plane.

3 The light field dynamics

3.1 Intracavity dynamics

For our purposes we consider here an ideal mode-degenerate-cavity, containing a $\chi^{(2)}$ crystal that is capable to convert a pump field $\mathcal{A}_\mathrm{p}$ of frequency $2\omega_\mathrm{s}$ into a signal field of frequency ω_s and *vice versa*. The crystal is located at the point C (see Fig. 1), midway between the two lenses L_1 and L_2, and is much shorter than the Rayleigh length of the resonator (or, equivalently, much shorter than the cavity length). The reference plane $z = 0$ is taken at the point C, and the cavity beam waist will be denoted by w_c.

For the signal beam we assume that the input/output mirror M_1 has a high reflectivity while all the others cavity mirrors are completely reflecting; hence the cavity has only one input-output port at the signal wavelength. Instead, for what concerns the pump field, we assume that the cavity mirrors are completely transparent at the pump frequency $2\omega_\mathrm{s}$; hence the pump simply travels once through the crystal. Moreover, below the threshold for parametric oscillations, the pump depletion can be neglected, and the coherent stationary pump field can be described by means of its classical amplitude $\mathcal{A}_\mathrm{p}(\boldsymbol{\rho})$. Notice that we allow for dependence of pump profile on the transverse coordinate.

In a ideal confocal resonator all the functions of the transverse coordinate having a given parity with respect

to the space inversion $\boldsymbol{\rho} \to -\boldsymbol{\rho}$ are transverse proper modes, that is, they transform into themselves (apart from a global phase factor) after one cavity round trip. Because of the cylindrical symmetry it is convenient to consider among them the Gauss-Laguerre modes [10] that have the following transverse configuration at the plane $z = 0$

$$f_{p,l,i}(\rho,\phi) = \frac{2}{\sqrt{2^{\delta_{l0}}\pi w_{\rm c}^2}}\sqrt{\frac{p!}{(p+l)!}}\left(2\frac{\rho^2}{w_{\rm c}^2}\right)^{\frac{l}{2}} L_p^l\left(2\frac{\rho^2}{w_{\rm c}^2}\right) \times \exp\left[-\frac{\rho^2}{w_{\rm c}^2}\right]\begin{cases}\cos(l\phi) & \text{for} \quad i=1\\ \sin(l\phi) & \text{for} \quad i=2\end{cases}, \quad (7)$$

with $p, l = 0, 1, 2, ...$ being the radial and angular indices of the mode, respectively. ρ and ϕ denote the radial and angular coordinates in the transverse plane, *i.e.* $\rho = |\boldsymbol{\rho}|$, and $\phi = \arg[\boldsymbol{\rho}]$. L_p^l stand for the Laguerre polynomials of the indicated argument. In an ideal confocal resonator the proper modes (longitudinal and transverse) gather into frequency degenerate families [10], characterized by the integer index $n = 2q + 2p + l$, where q (integer) is the longitudinal index. The frequency separation between the families is equal to one half the free spectral range.

We now assume that only one of these families, for definiteness one corresponding to l even, is close to the frequency of the signal field, while all the others are far away and do not contribute to the dynamics. Let us denote with $\omega_{\rm c}$ the frequency of the resonant mode family having the index $n = n_{\rm c}$; this family ideally contains an infinite number of even Gauss-Laguerre modes, that constitute a complete and orthonormal basis for any function of the transverse coordinates even with respect to coordinate inversion in the transverse plane.

Let us introduce the envelope operator of the intracavity field over the modes of the resonant family in the following way

$$B_+(\boldsymbol{\rho},t) = \sum_{p,l,i} f_{p,l,i}(\boldsymbol{\rho}) b_{p,l,i}(t), \quad \text{for } z = 0, \quad (8)$$

where the sum is extended to modes with an even parity, and $b_{p,l,i}(t)$ indicate mode operators, obeying the equal time commutation relations:

$$\left[b_{p,l,i}(t), b^\dagger_{p',l',i'}(t)\right] = \delta_{p,p'}\,\delta_{l,l'}\,\delta_{i,i'}\,. \quad (9)$$

We assume the validity of the mean field limit [11] which, together with the assumption of a short crystal, allows to consider the field B constant along the crystal length.

The Hamiltonian which governs the dynamics of the signal field in the cavity has two contributions. $H_{\rm free}$ describes the free evolution of the intracavity field

$$H_{\rm free}(\boldsymbol{\rho},t) = \hbar\sum_{p,l,i}^{l\,\text{even}}(\omega_{p,l,i}-\omega_s) b^\dagger_{p,l,i} b_{p,l,i} = \hbar(\omega_{\rm c}-\omega_{\rm s})\int {\rm d}\boldsymbol{\rho}\, B_+^\dagger(\boldsymbol{\rho},t) B_+(\boldsymbol{\rho},t), \quad (10)$$

where the rapid oscillation at frequency $\omega_{\rm s}$ has been eliminated. In writing (10) we have taken into account only the modes of the quasi-resonant family, for which $\omega_{p,l,i} = \omega_{\rm c}$ since the others are far off-resonance and therefore we will assume they are in the vacuum state in the absence of any input. The other contribution is given by $H_{\rm int}$ which describes the parametric interaction in the crystal

$$H_{\rm int}(\boldsymbol{\rho},t) = {\rm i}\hbar\frac{\gamma}{2}\int {\rm d}\boldsymbol{\rho}\mathcal{A}_{\rm p}(\boldsymbol{\rho})\left[B_+^\dagger(\boldsymbol{\rho},t)^2 - B_+(\boldsymbol{\rho},t)^2\right], \quad (11)$$

with $\mathcal{A}_{\rm p}$ being the classical amplitude of the pump field, scaled by the cavity bandwidth γ. Its dependence from the transverse position vector $\boldsymbol{\rho}$ takes into account the profile of the pump field which is assumed an even function of $\boldsymbol{\rho}$. In the case of a plane pump it becomes independent of $\boldsymbol{\rho}$. Without loss of generality we also assume $\mathcal{A}_{\rm p}(\boldsymbol{\rho})$ real.

In the framework of the input-output theory for open cavities [12], the intracavity field dynamics is described by the following Langevin equation

$$\frac{\partial}{\partial t}B_+(\boldsymbol{\rho},t) = -\gamma\left[(1+{\rm i}\Delta_+)B_+(\boldsymbol{\rho},t) - {\rm A_p}(\boldsymbol{\rho})B_+^\dagger(\boldsymbol{\rho},t)\right] + \sqrt{2\gamma}B_+^{\rm in}(\boldsymbol{\rho},t), \quad (12)$$

where $\Delta_+ = (\omega_{\rm c}-\omega_{\rm s})/\gamma$. Here $B_+^{\rm in}(\boldsymbol{\rho},t)$ denotes the part of the input field operator even with respect to the inversion of the transverse coordinate. More precisely we introduce even and odd input/output operators as

$$B_\pm^{\rm in/out}(\boldsymbol{\rho},t) = \frac{1}{2}\left[B^{\rm in/out}(\boldsymbol{\rho},t) \pm B^{\rm in/out}(-\boldsymbol{\rho},t)\right], \quad (13)$$

where for example $\boldsymbol{\rho}$ is in the upper semiplane. $B^{\rm in/out}$ represent the envelope operators of the input/output fields calculated at a fixed plane z, and obey the following commutation relations

$$\left[B_\pm^{\rm in/out}(\boldsymbol{\rho},t), B_\pm^{\rm in/out\dagger}(\boldsymbol{\rho}',t')\right] = \frac{1}{2}\Big[\delta(\boldsymbol{\rho}-\boldsymbol{\rho}') \pm \delta(\boldsymbol{\rho}+\boldsymbol{\rho}')\Big]\delta(t-t'), \quad (14)$$

$$\left[B_\pm^{\rm in/out}(\boldsymbol{\rho},t), B_\mp^{\rm in/out\dagger}(\boldsymbol{\rho}',t)\right] = 0. \quad (15)$$

Equation (12) amounts to an infinite set of uncoupled equations (one for each transverse point $\boldsymbol{\rho}$), describing single-mode optical parametric oscillators with the same frequency, (that of the even Gauss-Laguerre modes). The relation linking the outgoing fields $B_\pm^{\rm out}(\boldsymbol{\rho},t)$ with the intracavity and input fields at the cavity input/output port reads [12]

$$B_\pm^{\rm out}(\boldsymbol{\rho},t) = \sqrt{2\gamma}B_\pm(\boldsymbol{\rho},t) - B_\pm^{\rm in}(\boldsymbol{\rho},t), \quad (16)$$

Equation (12) can easily be solved in the frequency domain. Taking into account the relation (16) we obtain

$$B_+^{\rm out}(\boldsymbol{\rho},\Omega) = U(\boldsymbol{\rho},\Omega)B_+^{\rm in}(\boldsymbol{\rho},\Omega) + V(\boldsymbol{\rho},\Omega)B_+^{\rm in\dagger}(\boldsymbol{\rho},-\Omega), \quad (17)$$

where

$$B_{\pm}^{\mathrm{in/out}}(\boldsymbol{\rho},\Omega)=\int\frac{\mathrm{d}t}{\sqrt{2\pi}}B_{\pm}^{\mathrm{in/out}}(\boldsymbol{\rho},t)\mathrm{e}^{-\mathrm{i}\Omega t}, \tag{18}$$

and

$$U(\boldsymbol{\rho},\Omega)=\frac{\left[1-\mathrm{i}\left(\Delta_{+}-\overline{\Omega}\right)\right]\left[1-\mathrm{i}\left(\Delta_{+}+\overline{\Omega}\right)\right]+\mathcal{A}_{\mathrm{p}}^{2}(\boldsymbol{\rho})}{\left[1+\mathrm{i}\left(\Delta_{+}+\overline{\Omega}\right)\right]\left[1-\mathrm{i}\left(\Delta_{+}-\overline{\Omega}\right)\right]-\mathcal{A}_{\mathrm{p}}^{2}(\boldsymbol{\rho})}, \tag{19}$$

$$V(\boldsymbol{\rho},\Omega)=\frac{2\mathcal{A}_{\mathrm{p}}(\boldsymbol{\rho})}{\left[1+\mathrm{i}\left(\Delta_{+}+\overline{\Omega}\right)\right]\left[1-\mathrm{i}\left(\Delta_{+}-\overline{\Omega}\right)\right]-\mathcal{A}_{\mathrm{p}}^{2}(\boldsymbol{\rho})}, \tag{20}$$

with $\overline{\Omega}=\Omega/\gamma$. Notice that a simply phase shift relate the input/output odd part of the field, since we assumed that only intracavity modes with even parity give dynamical contributions, *i.e.* $B_{-}^{\mathrm{out}}(\boldsymbol{\rho},\Omega)=\mathrm{e}^{\mathrm{i}\psi}B_{-}^{\mathrm{in}}(\boldsymbol{\rho},\Omega)$.

3.2 Propagation of the light field

Each one of the lenses 1 and 2 provides the spatial Fourier transform of the object field, so that the input field calculated at the cavity center C is given by:

$$B_{\mathrm{in}}(\boldsymbol{\rho},t)\equiv a(-\boldsymbol{\rho},t)\,. \tag{21}$$

The lens L_3 provides the Fourier transform of the output field, so that the output field at plane P is:

$$\widetilde{B}_{\mathrm{out}}(\boldsymbol{\xi},t)=\frac{1}{\lambda f}\int\mathrm{d}\boldsymbol{\rho}'\,B_{\mathrm{out}}(\boldsymbol{\rho}',t)\exp\left[\mathrm{i}\frac{2\pi}{\lambda f}\boldsymbol{\rho}'\cdot\boldsymbol{\xi}\right], \tag{22}$$

with λ the signal wavelength. The fourth lens provides its transform; however, due to the presence of the finite size aperture in plane P, the field in the image plane I becomes

$$e(\boldsymbol{\rho},t)=\frac{1}{\lambda f}\int\mathrm{d}\boldsymbol{\xi}\,\exp\left[\mathrm{i}\frac{2\pi}{\lambda f}\boldsymbol{\rho}\cdot\boldsymbol{\xi}\right]\times\left\{\mathcal{P}(\boldsymbol{\xi})\widetilde{B}_{\mathrm{out}}(\boldsymbol{\xi},t)+\left[1-\mathcal{P}(\boldsymbol{\xi})\right]\widetilde{B}_{\mathrm{vac}}(\boldsymbol{\xi},t)\right\}, \tag{23}$$

where $\mathcal{P}(\boldsymbol{\xi})$ is equal to 1 in the pupil area and zero elsewhere (in addition we assume this function symmetrical, *i.e.* $\mathcal{P}(-\boldsymbol{\xi})=\mathcal{P}(\boldsymbol{\xi})$). In equation (23) an auxiliary field operator in the vacuum state $\widetilde{B}_{\mathrm{vac}}(\boldsymbol{\xi},t)$ has been introduced [2] in order to account for vacuum field fluctuations from the screen in plane P; this operator is necessary to preserve the commutation relation (14) for the field $e(\boldsymbol{\rho},t)$, but it gives no contribution to the normally ordered correlation functions in equations (2, 3), hence we shall omit it in what follows.

Now, by inserting equation (22) into (23), we obtain

$$e(\boldsymbol{\rho},t)=\frac{1}{\lambda f}\int\mathrm{d}\boldsymbol{\rho}'\,\wp(\boldsymbol{\rho}+\boldsymbol{\rho}')B_{\mathrm{out}}(\boldsymbol{\rho}',t), \tag{24}$$

where the function $\wp(\boldsymbol{\rho})$ is related to the pupil frame function as

$$\wp(\boldsymbol{\rho})=\frac{1}{\lambda f}\int\mathrm{d}\boldsymbol{\xi}\,\mathcal{P}(\boldsymbol{\xi})\exp\left[\mathrm{i}\frac{2\pi}{\lambda f}\boldsymbol{\xi}\cdot\boldsymbol{\rho}\right], \tag{25}$$

and represents the impulse response of the optical system. For infinitely large pupil $\wp(\boldsymbol{\rho})=\lambda f\delta(\boldsymbol{\rho})$, and $e(\boldsymbol{\rho},t)\equiv B_{\mathrm{out}}(-\boldsymbol{\rho},t)$.

Furthermore, by means of the relations (17, 21) we can write

$$e(\boldsymbol{\rho},\Omega)=\frac{1}{\lambda f}\int\mathrm{d}\boldsymbol{\rho}'\,\wp(\boldsymbol{\rho}+\boldsymbol{\rho}')\left[U(\boldsymbol{\rho}',\Omega)a_{+}(\boldsymbol{\rho}',\Omega)+V(\boldsymbol{\rho}',\Omega)a_{+}^{\dagger}(\boldsymbol{\rho}',-\Omega)\right]-\frac{1}{\lambda f}\int\mathrm{d}\boldsymbol{\rho}'\,\wp(\boldsymbol{\rho}+\boldsymbol{\rho}')\left[\mathrm{e}^{\mathrm{i}\psi}a_{-}(\boldsymbol{\rho}',\Omega)\right], \tag{26}$$

where $a_{\pm}$ are the even/odd part of the field in the object plane.

Finally, the optimum choice of the pupil area S_{p} can be done as follows. Let the input image of area S_{O}, have details (or image elements) of certain area $S_{\mathrm{el}}\ll S_{\mathrm{O}}$. Due to the presence of the pupil of area S_{p}, the optical system transforms a point source in the object plane in a diffraction pattern of area approximately equal to $S_{\mathrm{diff}}=(\lambda f)^2/S_{\mathrm{p}}$, which represents the minimum resolution area for an image (see *e.g.* [3] for more details). Thus we have to require:

$$S_{\mathrm{diff}}=\frac{(f\lambda)^2}{S_{\mathrm{p}}}<S_{\mathrm{el}}\,. \tag{27}$$

4 The amplified image and its fluctuations

In our analysis we shall restrict ourselves to stationary images. We assume that the field in the object plane is in a coherent state with its complex amplitude $s(\boldsymbol{\rho})$ modulated in space. This spatial modulation of the complex amplitude represents the input signal of the scheme or the image which is to be amplified.

For simplicity we now consider the situation where $s(\boldsymbol{\rho})$ is a real and even function of $\boldsymbol{\rho}$, while in Section 6 we shall consider a more general case. It follows from the stationarity of the input signal that

$$\langle a(\boldsymbol{\rho},\Omega)\rangle=\langle a_{+}(\boldsymbol{\rho},\Omega)\rangle=s(\boldsymbol{\rho})2\pi\delta(\Omega),\qquad\langle a_{-}(\boldsymbol{\rho},\Omega)\rangle=0\,. \tag{28}$$

Now, by using equations (26, 28) we can evaluate any normally ordered correlation function of the field operators in the image plane. However, to obtain explicit analytical results we make a further assumption. Since the typical linear spatial scale of change of the impulse response function is $S_{\mathrm{diff}}^{1/2}=\lambda f/S_{\mathrm{p}}^{1/2}$, we suppose that this distance is much smaller than the typical scale of change of U, V as well as of the input signal s. This allows us to take the latter functions out of the integral when they enter as a product with the impulse response function.

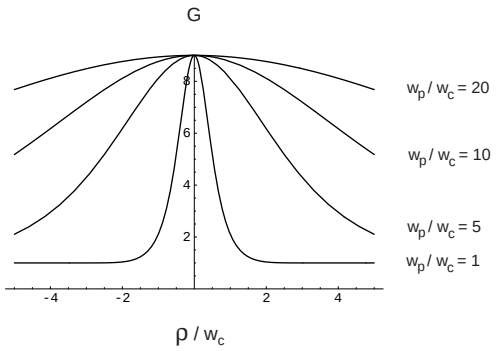

Fig. 2. Gain G (Eq. (31)) as a function of transverse distance ρ for different values of the pump waist. Here the pump has a Gaussian profile $\mathcal{A}_{\rm p}(\boldsymbol{\rho}) = 0.5\exp[-\rho^2/w_{\rm p}^2]$, and we assume perfect resonance $\Delta_+ = 0$.

Then, let us calculate the mean irradiance. We obtain

$$\langle e^\dagger(\boldsymbol{\rho},t)e(\boldsymbol{\rho},t)\rangle = s^2(\boldsymbol{\rho})\,|U(\boldsymbol{\rho},0)+V(\boldsymbol{\rho},0)|^2 + \frac{S_{\rm p}}{(\lambda f)^2}\frac{1}{2\pi}\int {\rm d}\Omega\;|V(\boldsymbol{\rho},\Omega)|^2\,. \quad (29)$$

The first term in equation (29) gives the amplified signal, while the second one describes the spontaneous fluorescence photon contribution. This contribution is finite provided the pupil has a finite area $S_{\rm p}$, while it diverges when the area $S_{\rm p}$ grows infinitely. The reason for this divergence lies in the infinitely large spatial bandwidth of our system.

Now, to calculate the relevant physical quantities (4, 5), we make two additional simplifying assumptions. First we assume that the size of each pixel in the photodetection array is small compared to the spatial scale of variation of the output field, so that we can substitute integration over the pixel area by multiplication by $S_{\rm d}$, with $S_{\rm d} \geq S_{\rm diff}$ and with the impulse response function approximated by a delta function. Second, we consider an observation time $T_{\rm d}$ long compared with the inverse cavity bandwidth γ^{-1}, which is the characteristic time scale of our system.

From equations (4, 2, 29) we easily obtain the mean number of photoelectrons

$$\langle N_{\rm I}(\boldsymbol{\rho},t)\rangle = \eta S_{\rm d}T_{\rm d}s^2(\boldsymbol{\rho})G(\boldsymbol{\rho}) + \eta\frac{S_{\rm p}S_{\rm d}}{(\lambda f)^2}\frac{T_{\rm d}}{2\pi}\int {\rm d}\Omega\;|V(\boldsymbol{\rho},\Omega)|^2\,, \quad (30)$$

where we have introduced the gain factor

$$G(\boldsymbol{\rho}) = |U(\boldsymbol{\rho},0)+V(\boldsymbol{\rho},0)|^2 = \left[\frac{1+\mathcal{A}_{\rm p}(\boldsymbol{\rho})}{1-\mathcal{A}_{\rm p}(\boldsymbol{\rho})}\right]^2, \quad (31)$$

considering the situation of perfect resonance, *i.e.* $\Delta_+ = 0$. Since in this model each point of the transverse plane represents an independent parametric oscillator whose gain is related to the strength of the pump in the same point, the spatial extent where the amplification takes places is determined by the pump size, as can be seen in Figure 2.

For the variance $\langle \Delta N_{\rm I}^2(\boldsymbol{\rho},t)\rangle$ we use equations (5, 3, 2, 26). Substituting $e(\boldsymbol{\rho},\Omega)$ from equation (26) into the intensity correlation function

$$\langle e^\dagger(\boldsymbol{\rho},t)e^\dagger(\boldsymbol{\rho}',t')e(\boldsymbol{\rho}',t')e(\boldsymbol{\rho},t)\rangle$$

in equation (3) we obtain sixteen mixed correlation functions of operators $a_+(\boldsymbol{\rho},\Omega)$ and $a_+^\dagger(\boldsymbol{\rho},\Omega)$ at four different points $\boldsymbol{\rho}$ and frequencies Ω (we recall that the terms containing $a_-(\boldsymbol{\rho},\Omega)$ give zero contribution). Using the commutator (14) we bring them to the normal order and then average over the coherent state of the input field. As a result we obtain two different kinds of terms: the first arises from interference of the amplified signal with the noise from spontaneous parametric radiation, and the second from self-interaction of this noise.

Finally we arrive at the following result:

$$\langle \Delta N_{\rm I}^2(\boldsymbol{\rho},t)\rangle = \langle N_{\rm I}(\boldsymbol{\rho},t)\rangle + \eta^2 S_{\rm d}T_{\rm d}g(S_{\rm d})s^2(\boldsymbol{\rho})G(\boldsymbol{\rho})\left\{G(\boldsymbol{\rho})-1\right\} + \eta^2\frac{S_{\rm p}S_{\rm d}}{(\lambda f)^2}\frac{T_{\rm d}}{2\pi}\int {\rm d}\Omega\;|V(\boldsymbol{\rho},\Omega)|^2\left[1+2\,|V(\boldsymbol{\rho},\Omega)|^2\right], \quad (32)$$

where the geometrical factor $g(S_{\rm d})$ is defined as:

$$g(S_{\rm d}) = \frac{1}{S_{\rm d}}\int_{S_{\rm d}}{\rm d}\boldsymbol{\rho}\int_{S_{\rm d}}{\rm d}\boldsymbol{\rho}'\frac{1}{2}\left[\delta(\boldsymbol{\rho}-\boldsymbol{\rho}')+\delta(\boldsymbol{\rho}+\boldsymbol{\rho}')\right]. \quad (33)$$

Clearly, for a symmetric detection region, which for example corresponds to detecting photons from two symmetric pixels in the image plane, $g(S_{\rm d}) = 1$; on the other side detection of photons from a single pixel in the image plane corresponds to $g(S_{\rm d}) = 1/2$. The term $\langle N_{\rm I}(\boldsymbol{\rho},t)\rangle$ in equation (32) represents the shot noise level, that is, the noise associated to a coherent state with the same mean intensity. In the remaining part of the formula, the term proportional to $\eta^2 s^2(\boldsymbol{\rho})G(\boldsymbol{\rho})$ stems from the interference of the amplified signal with noise and the other quadratic in η from the self interference of the noise. This latter determines the inherent noise of the amplifier present even without the signal on its input.

5 Conditions for noiseless amplification

Let us first consider the mean number of detected photoelectrons given by equation (30). It contains two contributions. The first one, proportional to the intensity $s^2(\boldsymbol{\rho})$ of the input image at the point $\boldsymbol{\rho}$, carries all the information about the amplified image. The second term does exist even when no signal is present at the input. Its physical origin is in the phenomenon of spontaneous parametric down-conversion. For a large pump spot size, the function $V(\boldsymbol{\rho},\Omega)$ can be assumed almost flat over the region when the image is non zero. Hence, this term gives a contribution approximately uniform over the image region; however this contribution increases with the pupil size $S_{\rm p}$ at the expenses of the visibility of the amplified image. This imposes a lower limit on the intensity of the input

signal $s(\boldsymbol{\rho})$ that can be amplified without adding noise. Indeed, one can neglect the spontaneously down converted photons compared to the amplified signal if

$$s^2(\boldsymbol{\rho})G(\boldsymbol{\rho}) \gg \frac{1}{S_{\rm diff}}\frac{1}{2\pi}\int \mathrm{d}\Omega\ |V(\boldsymbol{\rho},\Omega)|^2\,. \qquad (34)$$

In the case of high gain, $G \gg 1$, we have $|U| \simeq |V| \gg 1$, and $G \simeq 4|V|^2$. By approximating $\int \mathrm{d}\Omega\, |V(\boldsymbol{\rho},\Omega)|^2 \approx \gamma |V(\boldsymbol{\rho},0)|^2$ condition (34) can be rewritten as

$$s^2(\boldsymbol{\rho})S_{\rm diff}T_{\rm amp} \gg 1/4, \qquad (35)$$

where we have introduced the typical temporal scale of the system as $T_{\rm amp} = 2\pi/\gamma$.

Analogously, a condition for noiseless amplification arises from equation (32) for dispersion of the observed number of photoelectrons. Namely, the self-interference term in equation (32), given by the last integral, must be small compared to the term due to the interference of the amplified signal with noise, *i.e.* the term proportional to $\eta^2 s^2(\boldsymbol{\rho})G(\boldsymbol{\rho})$. This gives, provided $S_{\rm d} > S_{\rm diff}$,

$$s^2(\boldsymbol{\rho})S_{\rm diff}T_{\rm amp} \gg 1/8, \qquad (36)$$

which for the order of magnitude is equivalent to condition (35).

Let us now consider the situation of a symmetric detection region in the image plane (that is $g(S_{\rm d}) = 1$). When conditions (35, 36) are fulfilled the signal-to-noise ratio of the amplified image is given by using equations (6, 30, 32), obtaining

$$R_{\rm I} = \frac{\eta S_{\rm d}T_{\rm d}s^2(\boldsymbol{\rho})G(\boldsymbol{\rho})}{1+\eta\,[G(\boldsymbol{\rho})-1]}\,. \qquad (37)$$

Furthermore, to study quantitatively the noise performance of the amplifier we introduce the noise figure F as

$$F = \frac{R_{\rm O}(\eta=1)}{R_{\rm I}}\,. \qquad (38)$$

Since a linear amplifier cannot improve the signal-to-noise ratio in the input image, the noise figure is always not smaller than unity. We refer to the case $F = 1$ as *noiseless amplification*. Notice that in equation (38) the input signal-to-noise ratio refers to ideal photodetection in the input plane. As explained on reference [2], this condition is necessary to obtain the noise figure characterizing the noise added by the amplifier, but not the noise in the pre-amplification stage (like non-ideal photodetection in the object plane). Without such correction, *i.e.* allowing for non-ideal photodetection in the object plane with $\eta < 1$, one could obtain a noise figure smaller than unity. The physical features of this phenomenon lies in the fact that noiseless amplifier can compensate the imperfection of the photodetection scheme on the pre-amplification stage and formally "improve" the signal-to-noise ratio of the input image degradated by non-ideal photodetection array.

The signal-to-noise ratio in the object plane is defined in analogy to (6). Since

$$\langle N_{\rm O}(\boldsymbol{\rho},t)\rangle = S_{\rm d}T_{\rm d}s^2(\boldsymbol{\rho}),\ \langle \Delta N_{\rm O}^2(\boldsymbol{\rho},t)\rangle = S_{\rm d}T_{\rm d}s^2(\boldsymbol{\rho}), \qquad (39)$$

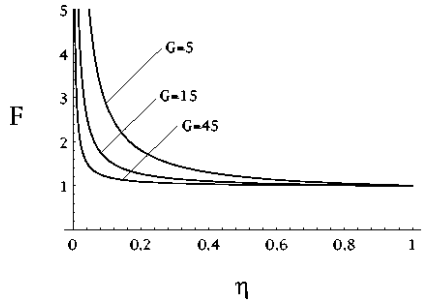

Fig. 3. Noise figure F (Eq. (41)) as a function of the quantum efficiency η for different values of the gain, for a symmetric detection region in the image plane. Here $\Delta_+ = 0$.

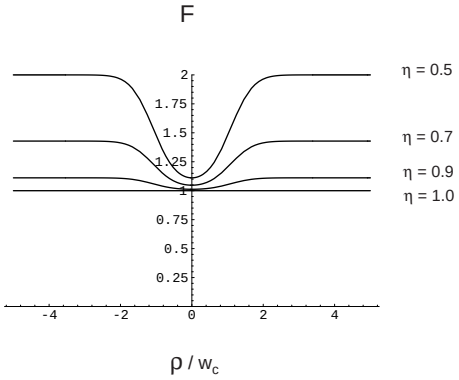

Fig. 4. Noise figure F (Eq. (41)) as a function of transverse distance ρ for different values of quantum efficiency. The pump profile is given by: $\mathcal{A}_{\rm p}(\boldsymbol{\rho}) = 0.5\exp[-\rho^2/w_{\rm c}^2]$, and $\Delta_+ = 0$.

we find

$$R_{\rm O} = \frac{\langle N_{\rm O}(\boldsymbol{\rho},t)\rangle^2}{\langle \Delta N_{\rm O}^2(\boldsymbol{\rho},t)\rangle} = S_{\rm d}T_{\rm d}s^2(\boldsymbol{\rho}). \qquad (40)$$

With the aid of equations (37, 40) we obtain

$$F = \frac{1}{\eta}\frac{\{1-\eta+\eta G(\boldsymbol{\rho})\}}{G(\boldsymbol{\rho})}\,. \qquad (41)$$

It may be seen that the ideal value of $F = 1$ is reached with any gain (satisfying the conditions (35, 36)) when $\eta = 1$. On the other side, for $\eta < 1$, the gain should be increased to compensate the effect of non efficient detection as shown in Figure 3.

It is also worth noting that the noise figure becomes independent from the vector position $\boldsymbol{\rho}$, that is, independent from the pump profile, when η approaches unity (Fig. 4).

Incidentally, if consider detection of light from a single pixel in the image plane (that is $g(S_{\rm d}) = 0.5$), it can be shown that equation (41) still holds given that η is replaced by $\eta/2$. Hence it results the possibility of noiseless amplification only for high gain, since detection from a single pixel corresponds to the case of not perfect efficiency stated above.

6 Beyond the ideal case

Till now we used a set of assumptions tailored to get the best and simplest results. However, in practical situations many of these hypothesis are not completely fulfilled. Hence we shall investigate what happens beyond the ideal case. First, we assumed that the pump and the signal were exactly locked in phase (for definiteness we assumed both of them real); however in practical situations a perfect locking of the two phases could be difficult to achieve. In order to allow for a phase mismatch between signal and pump, it is sufficient to make the replacement:

$$U(\boldsymbol{\rho},\Omega) \to U(\boldsymbol{\rho},\Omega)\mathrm{e}^{\mathrm{i}\zeta(\boldsymbol{\rho})}; \quad V(\boldsymbol{\rho},\Omega) \to V(\boldsymbol{\rho},\Omega)\mathrm{e}^{-\mathrm{i}\zeta(\boldsymbol{\rho})}, \tag{42}$$

where $\zeta = \arg[s] - \arg[\mathcal{A}_\mathrm{p}]/2$ represents the phase mismatch between the two fields. We allow for the possibility to have such a mismatch dependent on the transverse vector position.

Then, we introduce the phase sensitive gain G_φ as

$$\begin{aligned} G_\varphi(\boldsymbol{\rho}) &= \left|U(\boldsymbol{\rho},0)\mathrm{e}^{\mathrm{i}\zeta(\boldsymbol{\rho})} + V(\boldsymbol{\rho},0)\mathrm{e}^{-\mathrm{i}\zeta(\boldsymbol{\rho})}\right|^2 \\ &= \cos^2\varphi(\boldsymbol{\rho})\mathrm{e}^{2R(\boldsymbol{\rho})} + \sin^2\varphi(\boldsymbol{\rho})\mathrm{e}^{-2R(\boldsymbol{\rho})}, \end{aligned} \tag{43}$$

where the squeezing parameter $R(\boldsymbol{\rho})$ and the orientation angle $\varphi(\boldsymbol{\rho})$ are given by

$$\exp\left[\pm R(\boldsymbol{\rho})\right] = \left|U(\boldsymbol{\rho},0)\right| \pm \left|V(\boldsymbol{\rho},0)\right|, \tag{44}$$

$$2\varphi(\boldsymbol{\rho}) = \arg\left[U(\boldsymbol{\rho},0)\right] - \arg\left[V(\boldsymbol{\rho},0)\right] + 2\zeta(\boldsymbol{\rho}). \tag{45}$$

Repeating step by step the derivation of the noise figure, we get the more complete expression:

$$F = \frac{1}{\eta}\frac{\left\{1-\eta+\eta\left[\cos^2\theta(\boldsymbol{\rho})\mathrm{e}^{2R(\boldsymbol{\rho})} + \sin^2\theta(\boldsymbol{\rho})\mathrm{e}^{-2R(\boldsymbol{\rho})}\right]\right\}}{\left\{\cos^2\varphi(\boldsymbol{\rho})\mathrm{e}^{2R(\boldsymbol{\rho})} + \sin^2\varphi(\boldsymbol{\rho})\mathrm{e}^{-2R(\boldsymbol{\rho})}\right\}}, \tag{46}$$

with

$$\begin{aligned} 2\theta(\boldsymbol{\rho}) = 2\arg&\left[U(\boldsymbol{\rho},0)\mathrm{e}^{\mathrm{i}\zeta(\boldsymbol{\rho})} + V(\boldsymbol{\rho},0)\mathrm{e}^{-\mathrm{i}\zeta(\boldsymbol{\rho})}\right] \\ &- \arg\left[U(\boldsymbol{\rho},0)\right] - \arg\left[V(\boldsymbol{\rho},0)\right]. \end{aligned} \tag{47}$$

Figure 5 shows the behavior of the noise figure and the gain as functions of the phase mismatch between the pump (assumed here with a flat profile) and the signal field.

Another element that may degrade the performances of the scheme is a non perfect tuning of the cavity; so far we assumed exact resonance, which implies that the maximum gain throughout the transverse plane is achieved for a zero phase mismatch between pump and signal. Figure 6 plots F and G *versus* the cavity detuning, for a flat pump profile, and $\zeta = 0$. It should be noted that when $\Delta_+ \neq 0$, the value of the phase mismatch ζ that optimizes the gain and noise figure is different from zero, and changes from point to point if the pump is not flat; however when the pump profile varies slowly over the transverse plane, the optimal phase mismatch can be chosen to give the maximum gain at $\rho = 0$.

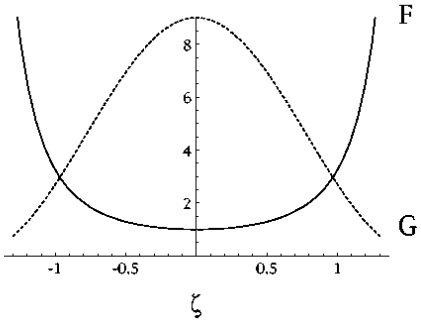

Fig. 5. Noise figure F (Eq. (46)) and gain G (Eq. (43)) as functions of phase difference ζ between pump and signal field. Here, the pump has a flat profile with amplitude $\mathcal{A}_\mathrm{p} = 0.5$, the quantum efficiency is $\eta = 1$, and $\Delta_+ = 0$.

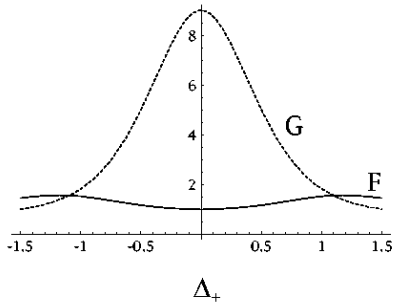

Fig. 6. Noise figure F (Eq. (46)) and gain G (Eq. (43)) as functions of the cavity detuning Δ_+. The pump is chosen flat with amplitude $\mathcal{A}_\mathrm{p} = 0.5$. Furthermore, $\zeta = 0$ and $\eta = 1$.

From the above figures we may infer that the performances of the scheme are not so much sensitive to problems like cavity tuning or phase control.

Now, let us focus on the problem of non perfect confocality. A slight deviation from the confocal geometry removes the mode degeneracy, and causes the frequencies of the modes belonging to the quasi-resonant family to depend on the transverse index $2p + l$; as a consequence the cavity detuning of the even Gauss-Laguerre modes takes on the form:

$$\Delta_{pl} = \Delta_+ + (2p + l + 1)\epsilon\,. \tag{48}$$

where the non-confocality parameter ϵ is given by (see *e.g.* [13])

$$\epsilon = \frac{\Lambda}{2\gamma}\left[\frac{4}{\pi}\tan^{-1}\left(\frac{d}{\sqrt{d(2R-d)}}\right) - 1\right], \tag{49}$$

where Λ denotes the free spectral range of the resonator; d is the distance between the two spherical mirrors of radius of curvature R in the case of a quasi-confocal Fabry-Perot resonator, or the distance between the two lenses of focal length $f = R/2$ in the equivalent ring-cavity configuration (shown in Fig. 1). The perfect confocal geometry corresponds to $R = d$, that is, $\epsilon = 0$; a small deviation from

the ideal case can be introduced by taking $R = d + \delta R$, with $|\delta R/d| \ll 1$. By keeping only the leading order in $\delta R/d$ in equation (49), the parameter of non-confocality can be expressed as:

$$\epsilon \approx -\frac{\Lambda}{\pi\gamma}\frac{\delta R}{d}\cdot \tag{50}$$

This shows that, provided $\delta R/d$ is small enough, a large number of even Gauss-Laguerre modes are much closer to the resonance frequency ω_s than the next family of modes, whose frequency is half a free spectral range apart; hence we are still allowed to take into account in our model only the modes of the quasi-resonant family. By exploiting the field expansion (8) it is possible to obtain a set of Langevin equations governing the dynamics of the mode amplitude operators. In the case of a flat pump profile, such equations are decoupled, and analytical calculations of the input/output relations can be performed for each mode. Turning back to spatial coordinates, and considering an infinite aperture in plane P, operators in the image plane result linked to those in the object plane by the following transformation:

$$B_+^{\rm out}(\boldsymbol{\rho},\Omega) = \int \mathrm{d}\boldsymbol{\rho}' \big[\mathcal{U}(\boldsymbol{\rho},\boldsymbol{\rho}',\Omega)B_+^{\rm in}(\boldsymbol{\rho}',\Omega) + \mathcal{V}(\boldsymbol{\rho},\boldsymbol{\rho}',\Omega)B_+^{\rm in\dagger}(\boldsymbol{\rho}',-\Omega)\big], \tag{51}$$

where the kernels of the integral are given by:

$$\mathcal{U}(\boldsymbol{\rho},\boldsymbol{\rho}',\Omega) = {\sum_{p,l,i}}' f_{p,l,i}(\boldsymbol{\rho})U_{p,l}(\Omega)f_{p,l,i}(\boldsymbol{\rho}'), \tag{52}$$

and

$$\mathcal{V}(\boldsymbol{\rho},\boldsymbol{\rho}',\Omega) = {\sum_{p,l,i}}' f_{p,l,i}(\boldsymbol{\rho})V_{p,l}(\Omega)f_{p,l,i}(\boldsymbol{\rho}'). \tag{53}$$

Here $U_{p,l}(\Omega)$ and $V_{p,l}(\Omega)$ are given by equations (19, 20) with the replacement $\Delta_+ \to \Delta_{p,l}$.

From equation (51) we can notice that the first effect of a deviation from perfect confocality is to introduce a finite resolution in the amplification scheme: the device is not able to resolve details of the input image on a length scale smaller than the scale of variation of the kernels of the integral (51).

It can be noticed that in the confocal limit $\epsilon \to 0$, $U_{p,l}$ and $V_{p,l}$ do not depend on the modal index and can be extracted from the sums (52, 53). The completeness of the mode set for the even functions of $\boldsymbol{\rho}$ then leads to

$$\lim_{\epsilon\to 0}\mathcal{U}(\boldsymbol{\rho},\boldsymbol{\rho}',\Omega) = U(\Omega)\frac{1}{2}\left[\delta(\boldsymbol{\rho}-\boldsymbol{\rho}') + \delta(\boldsymbol{\rho}+\boldsymbol{\rho}')\right], \tag{54}$$

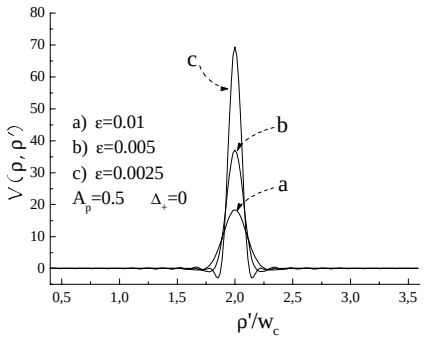

Fig. 7. Case of non-perfect confocality. The convolution kernel $\mathcal{V}(\boldsymbol{\rho},\boldsymbol{\rho}',\Omega=0)$ is plotted as a function of the second point along the radial direction ρ', scaled to the cavity waist w_c; $\rho = 2w_c$ and the angular coordinates of the two points coincide. The three curves correspond to (a) $\epsilon = 10^{-2}$, (b) $\epsilon = 0.5\times10^{-2}$, (c) $\epsilon = 0.25\times10^{-2}$; $\mathcal{A}_p = 0.5$, $\Delta_+ = 0$.

and a similar expression for $\mathcal{V}$. Thus for ϵ small but finite we may expect the integral kernels to be strongly peaked around $\boldsymbol{\rho}' = \pm\boldsymbol{\rho}$. This is actually the case, as shown by Figure 7, which gives an example of the scale of variation of $\mathcal{V}$ along the radial coordinate, for decreasing values of the non-confocality parameter; values of ϵ smaller than 0.2×10^{-2} are unfortunately not accessible to numerical calculations, because the routines that generate the Gauss-Laguerre modes become unstable at very high modal orders.

To proceed on with explicit calculations, we now assume that the input image has a scale of variation much larger than that of $\mathcal{V}$, $\mathcal{U}$, so that the all the quantities referring to the input signal can be extracted from the integral sign in (51). This allows us to evaluate the gain function as:

$$\mathcal{G}(\boldsymbol{\rho}) = \left|\mathcal{I}_{\mathcal{U}}(\boldsymbol{\rho})\mathrm{e}^{\mathrm{i}\zeta(\boldsymbol{\rho})} + \mathcal{I}_{\mathcal{V}}(\boldsymbol{\rho})\mathrm{e}^{-\mathrm{i}\zeta(\boldsymbol{\rho})}\right|^2, \tag{55}$$

where we have introduced

$$\mathcal{I}_{\mathcal{U}}(\boldsymbol{\rho}) = \int \mathrm{d}\boldsymbol{\rho}'\mathcal{U}(\boldsymbol{\rho},\boldsymbol{\rho}',0) = \sqrt{2\pi}\sum_p f_{p,0,1}(\boldsymbol{\rho})(-1)^p U_{p,0}(0), \tag{56}$$

and

$$\mathcal{I}_{\mathcal{V}}(\boldsymbol{\rho}) = \int \mathrm{d}\boldsymbol{\rho}'\mathcal{V}(\boldsymbol{\rho},\boldsymbol{\rho}',0) = \sqrt{2\pi}\sum_p f_{p,0,1}(\boldsymbol{\rho})(-1)^p V_{p,0}(0). \tag{57}$$

The noise figure results as

see equation (58) below.

$$\mathcal{F}(\boldsymbol{\rho}) = \frac{\mathcal{G}(\boldsymbol{\rho}) + 2\eta\left\{|\mathcal{I}_{\mathcal{V}}(\boldsymbol{\rho})|^2\mathcal{G}(\boldsymbol{\rho}) + \mathrm{Re}\left\{\mathcal{I}_{\mathcal{V}}(\boldsymbol{\rho})\mathcal{I}_{\mathcal{U}}(\boldsymbol{\rho})\left[\mathcal{I}^*_{\mathcal{U}}(\boldsymbol{\rho})\mathrm{e}^{-\mathrm{i}\zeta(\boldsymbol{\rho})} + \mathcal{I}^*_{\mathcal{V}}(\boldsymbol{\rho})\mathrm{e}^{\mathrm{i}\zeta(\boldsymbol{\rho})}\right]^2\right\}\right\}}{\eta\mathcal{G}^2(\boldsymbol{\rho})} \tag{58}$$

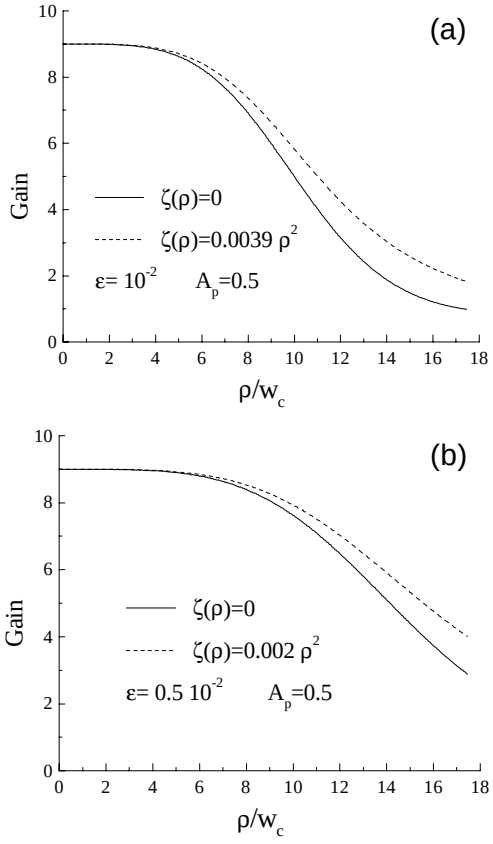

Fig. 8. Case of non perfect confocality. The gain $\mathcal{G}$ (Eq. (55)) is plotted *versus* the distance from the axis of the scheme, for (a) $\epsilon = 10^{-2}$ and (b) $\epsilon = 0.5 \times 10^{-2}$. Solid lines: input signal and pump have flat wavefronts with a phase mismatch $\zeta = 0$; dashed lines refer to a signal input phase quadratic in the radial coordinate. The pump profile is flat, with amplitude $\mathcal{A}_\mathrm{p} = 0.5$, $\eta = 1$, and $\Delta_+ = 0$.

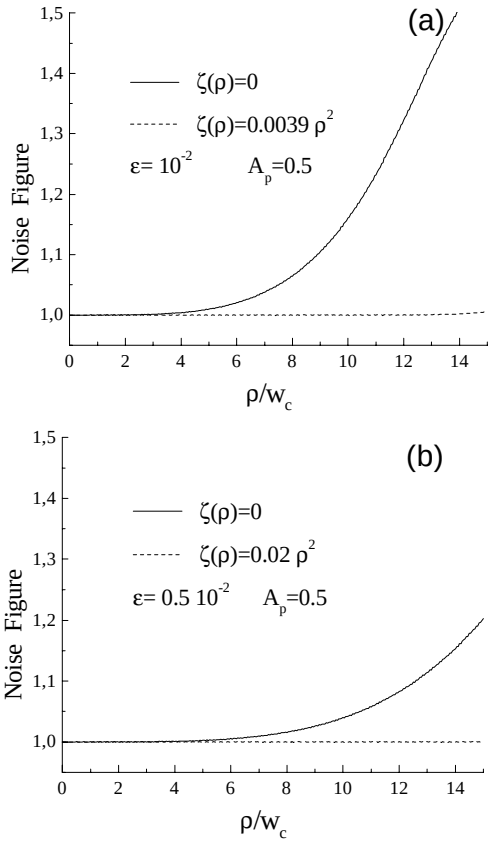

Fig. 9. Case of non perfect confocality. Noise figure *versus* distance from the optical axis. Solid lines: input signal and pump have flat wavefronts and the same phase; dashed lines: the input signal has a quadratic wavefront. Other parameters as in Figure 8.

Figures 8a and 8b plot the gain $\mathcal{G}$ as a function of the distance from the optical axis, scaled to the cavity waist, for two different values of the non-confocality parameter ϵ, and for a flat pump profile. The solid lines correspond to both pump and input signal having a flat wavefront, with the constant phase mismatch ζ chosen in order to optimize the gain for $\rho = 0$. In comparison with the ideal confocal case, the gain is no more uniform over the transverse plane, and the size of the region of the input image that can be amplified decreases as the non-confocality parameter ϵ increases, that is, with increasing deviation from the confocal geometry. However, by comparison with Figure 7, the size of the amplified region results large compared to the resolution length (the width of the peaks in Fig. 7); thus when departures from the confocal geometry are small, a still large number of input image pixels can be efficiently amplified.

The reasons why the gain is not uniform are basically the following:

1. the available gain is not distributed in a uniform way among the modes, because, when ϵ is not zero, high order modes are off-resonance, and hence are not amplified by the device. In regions far away from the optical axis only high order Gauss-Laguerre modes give a non-vanishing contribution, and hence these regions of the input image are not amplified;
2. the amplification undergone by each mode is sensitive to the phase mismatch ζ; a fixed phase mismatch maximizes the gain for modes corresponding to a given index $2p + l$. For example, in the plot, the choice $\zeta = 0$ optimizes the gain for the TEM_{00} mode, but not for high order modes.

There is however a way to partially compensate for the second effect; indeed it turns out that a quadratic input wavefront may result in a increase of the gain in points far away from the optical axis, as shown by the dashed lines in Figure 8.

If, on the one side, the improvement obtained in this way for what concerns the gain is rather marginal, on the other the noise figure of the amplifier benefits in a substantial way from this kind of arrangement. Figures 9a and 9b plot the noise figure as a function of the radial coordinate in the transverse plane, under the same conditions as Figures 8a and 8b. The solid lines correspond to a flat input wavefront, while the dashed lines correspond to an input signal wavefront quadratic in ρ, and show that noiseless

amplification can be achieved in a almost uniform way over the transverse plane.

Clearly the curvature of the input wavefront must be carefully chosen in order to minimize the noise figure (maximize the gain); in the numerical calculations this choice is made by analysing the dependence on ρ of the function $\arg[\mathcal{I}_{\mathcal{U}}(\rho)] - \arg[\mathcal{I}_{\mathcal{V}}(\rho)]$. In an experimental realization a quadratic wavefront could be introduced by adjusting the optical scheme. For example, a displacement δz of the object plane away from the lens L1 gives the desired effect; in fact in such a case the propagation of the Gauss-Laguerre modes introduces a phase factor [13]

$$\arg\left[f_{p,l,i}\right] \approx \left[\frac{\rho^2}{w_{\mathrm{c}}^2}(1-\delta z) + (2p+l+1)\right]\delta z, \qquad (59)$$

that can partly compensate the degrading effects on the signal.

7 Conclusions

Summarizing, we have studied the confocal geometry for parametric image amplification in optical cavities. This scheme offers the possibility of amplifying a faint image at once, avoiding any scanning procedure. Moreover, its performances turn out to be not much fragile to experimental imperfections. The obtained results could be of interest in many areas of physics which would benefit from having a possibility of noiseless amplification of faint optical images.

We mention for example microscopy, which in this case would be able to widen the range of finest detectable objects, or bio-medical imaging, where it may be necessary to use low intensity light in order to avoid damage to tissues. An other field which comes to mind is that of astronomy, where, however, a problem is represented by the fact that the light coming from stars is not coherent.

References

1. J.A. Levenson, I. Abram, T. Rivera, P. Fayolle, J.C Garreu, Ph. Grangier, Phys. Rev. Lett. **70**, 267 (1993); J.A. Levenson, I. Abram, T. Rivera, Ph. Grangier, J. Opt. Soc. Am. B **10**, 2233 (1993).
2. M.I. Kolobov, L.A. Lugiato, Phys. Rev. A **52**, 4930 (1995).
3. I.V. Sokolov, M.I. Kolobov, L.A. Lugiato, Phys. Rev. A **60**, 2420 (1999).
4. A. Gatti, E. Brambilla, L.A. Lugiato, M. Kolobov, J. Opt. B: Quant. Semiclass. Opt. (in press).
5. F. Devaux, E. Lantz, A. Lacourt, D. Gindre, H. Maillotte, P.A. Doreau, T. Laurent, Nonlin. Opt. **11**, 25 (1995); F. Devaux, E. Lantz, Opt. Commun. **114**, 295 (1995); F. Devaux, E. Lantz, Opt. Commun. **118**, 25 (1995); F. Devaux, E. Lantz, J. Opt. Soc. Am. B **12**, 2245 (1995); S. M. Cameron, D.F. Bliss, M.W. Kimmell, Proc. SPIE **2679**, 195 (1996).
6. M.L. Marable, S.K. Choi, P. Kumar, Opt. Expr. **2**, 84 (1998).
7. Sang-Kyung Choi, Michael Vasilyev, Prem Kumar, Phys. Rev. Lett. **83**, 1938 (1999).
8. R.J. Glauber, Phys. Rev. **130**, 2529 (1963); *ibid.* **131**, 2766 (1963); P.L. Kelley, W.H. Kleiner, Phys. Rev. **136**, A316 (1964); D.F. Smirnov, A.S. Troshin, Sov. Phys. Usp. **30**, 851 (1987).
9. J.B. Thomas, *An Introduction to Statistical Communication Theory* (Wiley, New York, 1969); J.W. Goodman, *Statistical Optics* (Wiley, New York, 1985).
10. A.E. Siegman, *Lasers* (University Science, Mill Valley, CA 1986).
11. R. Bonifacio, L.A. Lugiato, Lett. Nuovo Cimento **21**, 505 (1978).
12. C.W. Gardiner, M.J. Collett, Phys. Rev. A **31**, 3761 (1985).
13. A. Yariv, *Quantum Electronics* (Wiley, New York, 1988), pp. 136–146.